Euro. Jnl of Applied Mathematics (2013), *vol.* 24, *pp.* 213–230.
doi:10.1017/S0956792512000381

Waveless subcritical flow past symmetric bottom topography

R. J. HOLMES[1], G. C. HOCKING[1], L. K. FORBES[2] and N. Y. BAILLARD[3]

[1]*Department of Mathematics and Statistics, Murdoch University, Perth, Western Australia*
emails: rachel.holmes.22@gmail.com, G.Hocking@murdoch.edu.au
[2]*School of Mathematics and Physics, University of Tasmania, Hobart, Australia*
email: Larry.Forbes@utas.edu.au
[3]*Bureau of Meteorology, Perth, Western Australia*
email: N.Baillard@bom.gov.au

(*Received 21 April 2012; revised 10 October 2012; accepted 10 October 2012; first published online 9 November 2012*)

The subcritical flow of a stream over a bottom obstruction or depression is considered with particular interest in obtaining solutions with no downstream waves. In the linearised problem this can always be achieved by superposition of multiple obstructions, but it is not clear whether this is possible in a full nonlinear problem. Solutions computed here indicate that there is an effective nonlinear superposition principle at work as no special shape modifications were required to obtain wave-cancelling solutions. Waveless solutions corresponding to one or more trapped waves are computed at a range of different Froude numbers and are shown to provide a rather elaborate mosaic of solution curves in parameter space when both negative and positive obstruction heights are included.

Key words: Stream flow; Free-surface flow; Water waves; Potential flow

1 Introduction

We consider the classic problem of steady flow of an ideal fluid in a stream of finite depth that is disturbed by an obstruction on the bed. Upstream of this disturbance, the fluid is flowing at a uniform speed and as the fluid hits the obstruction, the free surface of the fluid is disturbed. In particular, our interest in this work is in those solutions for which the surface returns to its original level with no downstream waves. This requirement leads to an 'ant farm' diagram of traces in parameter space where such solutions exist. The patterns are more elaborate than one might expect and some interesting distortions to the trapped waves appear on some of the waveless branches, especially in flow over a depression or depressions.

Solutions to the linearised problem of flow past an arbitrary obstruction on the stream bed were developed by Lamb [17]. Since the work of Lamb [17], this general problem has been studied extensively, with summaries of different aspects of the problem given in review articles by Long [18] and Baines [1].

Solutions to the full nonlinear problem were obtained numerically by Forbes [8,9], who considered a semi-elliptical obstruction on the stream bed, and Forbes and Schwartz [12] and Vanden-Broeck [21], who computed nonlinear solutions for flow over a semi-circular obstruction. Forbes [11] also computed hydraulic fall flows over a semi-circular

obstruction, which were verified by comparison with the results of a laboratory experiment. Belward [2] computed fully nonlinear solutions for flow over two obstructions, but considered only the case with critical flow over the first obstruction and supercritical flow over the second obstruction.

Higgins *et al.* [13] obtained solutions for symmetric and asymmetric mountain shapes on the stream bed by using a series-solution method. Zhang and Zhu [22, 23] computed the flow over a semi-circular obstruction using a hodograph method and also computed the second-order perturbation solution for flow over a semi-circular trench, which they then compared with solutions to the full nonlinear problem.

Weakly nonlinear solutions have been found using long wave theory and the Korteweg-de Vries (KdV) equation. Pratt [19] conducted an experiment which considered steady flow over two obstructions. He compared the results with long wave theory and found that in some circumstances the theory would fail. Dias and Vanden-Broeck [6, 7] used the KdV theory to find critical solutions over a single obstruction, but these had waves upstream. They found that if they introduced a second obstruction, the waves would be trapped between the two obstructions. Binder *et al.* [3, 4] computed the flow over two triangular obstructions and then a single rectangular obstruction on the stream bed, using both nonlinear methods and the KdV theory. They commented that for subcritical flow, the downstream waves could be eliminated by adjusting the obstruction separation in the case of two triangles, or the length in the case of a rectangular obstruction. In both cases, however, there was no further investigation into parameter values that result in these solutions. Choi [5] used the KdV equation with a negative forcing term to calculate flows over a single semi-circular trench.

Of particular interest is the work of Forbes [9], who found nonlinear solutions for subcritical flow over a semi-elliptical obstruction on the stream bed with no downstream waves. Forbes [9] found that given a fixed Froude number F and ellipse height β, the ellipse half lengths α could be found for which waveless solutions exist. Forbes [9] computed the first four values of α for different ellipse heights, given $F = 0.5$, and plotted contours showing the ellipse dimensions for which waveless solutions exist. He found that the first and second nonlinear contours merged together at the limiting value of the ellipse height. These results were confirmed and extended by Hocking *et al.* [16], who showed that higher order contours also merged.

These waveless subcritical solutions are of interest and will be the main focus of this paper. We extend the work of Forbes [9] and Hocking *et al.* [16] by computing nonlinear solutions for flow over two obstructions and also flow over two trenches. Contours are found that show obstruction dimensions at which solutions have no waves downstream of the second obstruction. Some of these solutions have trapped waves between the obstructions and the contours form an interesting pattern in parameter space.

2 Problem formulation

We will consider the problem of a two-dimensional steady flow of an ideal fluid in a stream of finite depth, disturbed by some bottom topography $y = B(x)$. Upstream of the disturbance, the flow is uniform with depth h and speed c. The free surface of the fluid $y = \eta(x)$ is initially unknown and computed as part of the solution.

https://doi.org/10.1017/S0956792512000381 Published online by Cambridge University Press

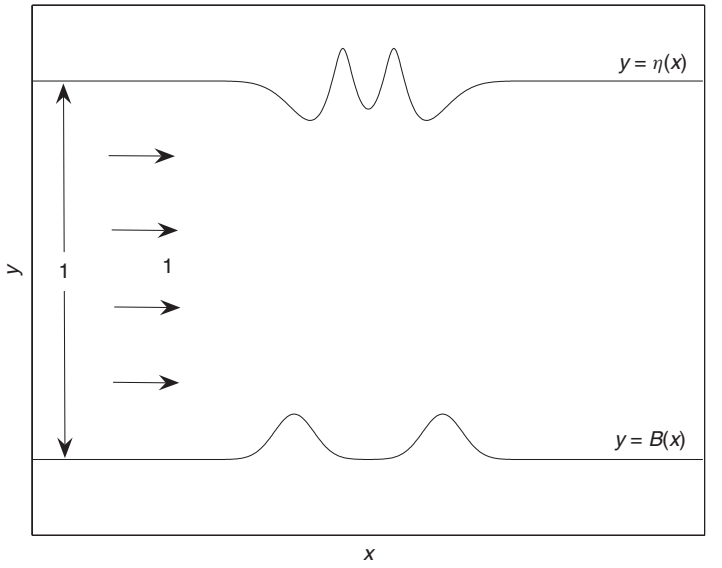

FIGURE 1. Diagram of the problem. Upstream of the obstruction, the flow is uniform with depth 1 and speed 1. The obstruction on the stream bed is given by $y = B(x)$ and on the unknown free surface by $y = \eta(x)$.

The assumption of a steady, two-dimensional flow of an ideal fluid allows us to define the velocity potential ϕ and requires that we solve Laplace's equation

$$\nabla^2\phi = 0 \tag{2.1}$$

subject to boundary conditions on the free surface and the stream bed.

We non-dimensionalise the problem with respect to the variables c and h. The flow then has an upstream speed of 1 and an upstream depth of 1. The dimensionless parameters of the flow are the dimensions of the obstruction and the non-dimensionalised flow rate, or Froude number,

$$F = \left(\frac{c^2}{gh}\right)^{\frac{1}{2}}. \tag{2.2}$$

A sketch of the non-dimensionalised problem can be seen in Figure 1.

There can be no flow normal to the surface of the fluid and also no flow normal to the stream bed, giving the conditions,

$$\eta'(x) = \frac{v}{u} \text{ on } y = \eta(x), \tag{2.3}$$

$$B'(x) = \frac{v}{u} \text{ on } y = B(x). \tag{2.4}$$

We also have the condition of constant pressure on the free surface which gives, from the Bernoulli equation,

$$\frac{1}{2}F^2(u^2 + v^2 - 1) + \eta = 1 \text{ on } y = \eta(x). \tag{2.5}$$

https://doi.org/10.1017/S0956792512000381 Published online by Cambridge University Press

3 Linearised problem

A solution to the linearised problem of an arbitrary shape on the stream bed is derived based on the work of Lamb [17] and applied to Gaussian-shaped obstructions. We consider the non-dimensionalised problem defined in the previous section, but instead take the undisturbed free surface at $y = 0$ and the unobstructed stream bed at $y = -1$.

The Bernoulli equation then gives,

$$\frac{1}{2}F^2(u^2 + v^2 - 1) + \eta = 0 \text{ on } y = \eta(x). \tag{3.1}$$

We have the conditions on the free surface and the stream bed,

$$u\eta'(x) = v \text{ on } y = \eta(x), \tag{3.2}$$

$$uB'(x) = v \text{ on } y = B(x). \tag{3.3}$$

We assume that the obstruction is small, $B(x) = -1 + B_1(x)$, and that the resulting disturbance is also small, $\phi = x + \Phi(x, y)$, where $\Phi(x, y)$ is a small perturbation to uniform flow. These assumptions allow us to obtain

$$F^2\frac{\partial \Phi}{\partial x} + \eta = 0 \text{ on } y = 0, \tag{3.4}$$

$$\eta'(x) = \frac{\partial \Phi}{\partial y} \text{ on } y = 0, \tag{3.5}$$

which combine to give,

$$F^2\frac{\partial^2 \Phi}{\partial x^2} + \frac{\partial \Phi}{\partial y} = 0 \text{ on } y = 0 \tag{3.6}$$

and we also have the condition on the stream bed in the form

$$\frac{\partial \Phi}{\partial y} = B_1'(x) \text{ on } y = -1. \tag{3.7}$$

An appropriate solution to Laplace's equation is

$$\Phi = \int_0^\infty [\alpha(k)\cosh ky + \beta(k)\sinh ky]\sin kx dk, \tag{3.8}$$

and we can find $\alpha(k)$ and $\beta(k)$ which satisfy the boundary conditions.

Assuming that $B_1'(x)$ can be written in the form

$$B_1'(x) = \int_0^\infty \gamma(k)\sin kx dk \tag{3.9}$$

and using conditions (3.6) and (3.7), we obtain

$$\alpha(k) = \frac{\gamma(k)}{F^2k^2\cosh k - k\sinh k}, \tag{3.10}$$

$$\beta(k) = \frac{F^2\gamma(k)}{F^2k\cosh k - \sinh k}. \tag{3.11}$$

https://doi.org/10.1017/S0956792512000381 Published online by Cambridge University Press

Rearranging (3.4) to give the free-surface elevation,

$$\eta = -F^2 \frac{\partial \Phi}{\partial x} \text{ on } y = 0 \tag{3.12}$$

and substituting Φ with $\alpha(k)$ and $\beta(k)$ as given above, we obtain

$$\eta = -\int_0^\infty \frac{\gamma(k)\cos kx}{k\cosh k - F^{-2}\sinh k} dk. \tag{3.13}$$

We consider a single Gaussian obstruction on the stream bed of height ε by taking,

$$B_1(x) = \varepsilon e^{-x^2}.$$

Then,

$$B_1'(x) = -2\varepsilon x e^{-x^2} \tag{3.14}$$

and we use an appropriate Fourier Sine Transform to obtain $\gamma(k)$ in the form,

$$\gamma(k) = -\frac{\varepsilon}{\sqrt{\pi}} k e^{-\frac{k^2}{4}}. \tag{3.15}$$

The surface elevation η is then

$$\eta = \frac{\varepsilon}{\sqrt{\pi}} \int_0^\infty \frac{k e^{-\frac{k^2}{4}} \cos kx}{k\cosh k - F^{-2}\sinh k} dk. \tag{3.16}$$

Using the same method as that used by Lamb [17], we obtain the free-surface elevation for subcritical Froude numbers as

$$\eta = -2\varepsilon\sqrt{\pi} \frac{\alpha^2 e^{-\frac{\alpha^2}{4}} \sin \alpha x}{\sinh \alpha(\alpha^2 + F^{-2} - F^{-4})} + \varepsilon\sqrt{\pi} \sum_{j=1}^{\infty} \frac{\beta_j^2 e^{\frac{\beta_j^2}{4}} e^{-\beta_j x}}{\sin \beta_j(\beta_j^2 - F^{-2} + F^{-4})} \text{ for } x > 0, \tag{3.17}$$

$$\eta = \varepsilon\sqrt{\pi} \sum_{j=1}^{\infty} \frac{\beta_j^2 e^{\frac{\beta_j^2}{4}} e^{\beta_j x}}{\sin \beta_j(\beta_j^2 - F^{-2} + F^{-4})} \text{ for } x < 0, \tag{3.18}$$

where α is the positive real root of the transcendental equation $\frac{\tanh \alpha}{\alpha} = F^2$ and the β_j, $j = 1, 2, 3, \ldots$ are imaginary roots.

The $e^{\beta_j^2}$ in the sum causes a problem when x is small. This means that the above solution is only valid far downstream.

To consider the case of two Gaussian obstructions on the stream bed, we take the first obstruction centred at $x = -b/2$ and the second obstruction centred at $x = b/2$. We are dealing with linear solutions, so we can simply superpose one solution onto the other,

https://doi.org/10.1017/S0956792512000381 Published online by Cambridge University Press

which gives

$$\eta = -2\varepsilon\sqrt{\pi}\frac{\alpha^2 e^{-\frac{\alpha^2}{4}}(\sin\alpha(x+\frac{b}{2})+\sin\alpha(x-\frac{b}{2}))}{\sinh\alpha(\alpha^2+F^{-2}-F^{-4})} + \varepsilon\sqrt{\pi}\sum_{j=1}^{\infty}\frac{\beta_j^2 e^{\frac{\beta_j^2}{4}}(e^{-\beta_j(x+\frac{b}{2})}+e^{-\beta_j(x-\frac{b}{2})})}{\sin\beta_j(\beta_j^2-F^{-2}+F^{-4})} \text{ for } x > \frac{b}{2}. \tag{3.19}$$

The first term gives the form of the waves downstream of the second Gaussian obstruction. We notice that there are zero waves downstream of the second obstruction when $\sin\alpha(x+\frac{b}{2})+\sin\alpha(x-\frac{b}{2}) = 0$, which occurs when the separation $b = \frac{(2k+1)\pi}{\alpha}$, $k = 0, 1, 2, \ldots$. We note that these values are independent of the height of the obstruction and also apply to obstructions of negative height, i.e. trenches. These separation values are evenly spaced, unlike the case of a semi-ellipse on the stream bed as considered by Forbes [8, 9] and Hocking *et al.* [16], where the waveless linearised solutions occur for ellipse lengths related to the zeros of a Bessel function.

4 Nonlinear problem and numerical methods

In order to solve a full nonlinear problem, we use a variation on the method of Forbes [10], in which the problem was formulated in the physical plane using arc length along the free surface as an independent variable. This method has been successfully applied in a number of different applications involving free-surface flows, see for example [6, 7, 14, 15].

We define a complex potential $f(z) = \phi + i\psi$, where $\psi(x, y)$ is the stream function. We consider the non-dimensionalised flow with the undisturbed free surface located at $y = 1$ and the unobstructed stream bed at $y = 0$, hence the streamline $\psi = 1$ corresponds to the free surface, $y = \eta(x)$, and the streamline $\psi = 0$ corresponds to the stream bed, $y = B(x)$.

The function $f'(z)$ is analytic, so we can apply Cauchy's integral formula for any fixed point on the boundary contour z_0,

$$f'(z_0) = \frac{1}{i\pi}\int_{\Gamma}\frac{f'(z)}{z-z_0}dz, \tag{4.1}$$

where $f'(z) = u - iv$, u and v are the horizontal and vertical components of the fluid velocity respectively, and Γ is the closed contour consisting of stream bed and free surface, connected by vertical lines at $x \to \pm\infty$. Taking the real part of this we obtain the equation for $u_0 = u(x_0, y_0)$,

$$u_0 = -\frac{1}{\pi}\int_{\Gamma}\frac{u[(y-y_0)-y'(x-x_0)]+v[(x-x_0)+y'(y-y_0)]}{(x-x_0)^2+(y-y_0)^2}dx. \tag{4.2}$$

The integral along the lines at $x = \pm\infty$ makes no contribution so that

$$u_0 = -\frac{1}{\pi}\int_{-\infty}^{\infty}\frac{u[(B-y_0)-B'(x-x_0)]+v[(x-x_0)+B'(B-y_0)]}{(x-x_0)^2+(B-y_0)^2}dx - \frac{1}{\pi}\int_{\infty}^{-\infty}\frac{u[(\eta-y_0)-\eta'(x-x_0)]+v[(x-x_0)+\eta'(\eta-y_0)]}{(x-x_0)^2+(\eta-y_0)^2}dx. \tag{4.3}$$

https://doi.org/10.1017/S0956792512000381 Published online by Cambridge University Press

In order to evaluate the integrals in equation (4.3), we truncate the domain at $x = \pm x_L$ and discretise the problem by taking $x_j = -x_L + (j-1)\frac{2x_L}{N-1}$, $j = 1, 2, \ldots, N$. We make an initial guess for each point on the free surface η_j, and the horizontal velocity at each point along the free surface and stream bed, u_{T_j} and u_{B_j} respectively, and evaluate equation (4.3) at each of the points (x_j, η_j) and (x_j, B_j), $j = 1, 2, \ldots, N$. The vertical velocities, v_{T_j} and v_{B_j}, are calculated using conditions (2.3) and (2.4).

When evaluating u_{B_j}, the first integral in (4.3) has a singularity at $x = x_0$ which can be removed by adding and subtracting terms as follows:

$$\begin{aligned} u_{B_j} = &-\frac{1}{\pi}\int_{-x_L}^{x_L} \frac{(u_B - u_{B_j})(\Delta B - B'\Delta x) + (v_B - v_{B_j})(\Delta x + B'\Delta B)}{\Delta x^2 + \Delta B^2} dx \\ &+ \left[\frac{u_{B_j}}{\pi} \arctan\frac{\Delta B}{\Delta x}\right]_{-x_L}^{x_L} - \left[\frac{v_{B_j}}{2\pi} \log[\Delta x^2 + \Delta B^2]\right]_{-x_L}^{x_L} \\ &- \frac{1}{\pi}\int_{x_L}^{-x_L} \frac{u_T((\eta - B_j) - \eta'\Delta x) + v_T(\Delta x + \eta'(\eta - B_j))}{\Delta x^2 + (\eta - B_j)^2} dx, \end{aligned} \tag{4.4}$$

where $\Delta x = x - x_j$ and $\Delta B = B - B_j$.

Similarly for u_{T_j} on the free surface,

$$\begin{aligned} u_{T_j} = &-\frac{1}{\pi}\int_{-x_L}^{x_L} \frac{u_B((B - \eta_j) - B'\Delta x) + v_B(\Delta x + B'(B - \eta_j))}{\Delta x^2 + (B - \eta_j)^2} dx \\ &- \frac{1}{\pi}\int_{x_L}^{-x_L} \frac{(u_T - u_{T_j})(\Delta\eta - \eta'\Delta x) + (v_T - v_{T_j})(\Delta x + \eta'\Delta\eta)}{\Delta x^2 + \Delta\eta^2} dx \\ &+ \left[\frac{u_{T_j}}{\pi} \arctan\frac{\Delta\eta}{\Delta x}\right]_{x_L}^{-x_L} - \left[\frac{v_{T_j}}{2\pi} \log[\Delta x^2 + \Delta\eta^2]\right]_{x_L}^{-x_L}, \end{aligned} \tag{4.5}$$

where $\Delta\eta = \eta - \eta_j$.

We find the error in these integral equations (4.4) and (4.5) along with the error in the Bernoulli equation (2.5) and iterate using Newton's method to find the free-surface elevation $y = \eta(x)$. The bottom surface $B(x)$ and its derivative $B'(x)$ are specified in advance, while the remaining derivatives are approximated using centred finite differences and the integrals approximated using the trapezoidal rule.

The majority of solutions considered will be for Gaussian obstructions of height ε and separation b, given by

$$B(x) = \varepsilon e^{-(x-b/2)^2} + \varepsilon e^{-(x+b/2)^2}. \tag{4.6}$$

We wish to find separation distances that result in zero waves downstream of the second obstruction. These can be found using the above method if we instead discretise the domain by $x_j = -x_L + (j-1)\frac{2x_L}{2N-1}$, $j = 1, 2, \ldots, 2N$ and specify symmetry, i.e. $\eta(x) = \eta(-x)$. We make an initial guess for b, η_j, u_{T_j} and u_{B_j}, $j = 1, 2, \ldots, 2N$. Fixing η_1, so we still have $3N$ equations in $3N$ unknowns, we iterate on the first N points and force symmetry about $x = 0$ at the beginning of each iteration.

For the computation of results in the following section, $N = 400$ points were used, corresponding to $2N = 800$ points across the free surface from $-x_L$ to x_L. Some test

https://doi.org/10.1017/S0956792512000381 Published online by Cambridge University Press

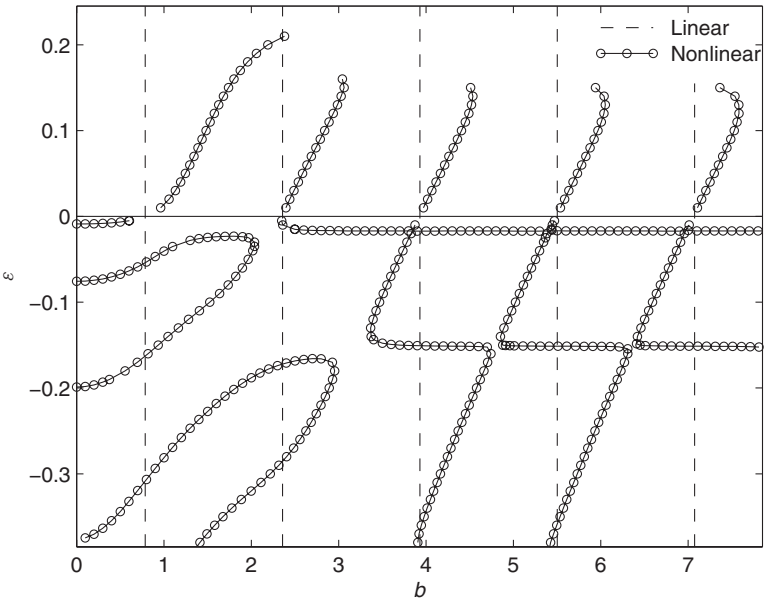

FIGURE 2. Contour plot showing the values of obstruction height and separation that result in waveless solutions for $F = 0.5$.

runs were done using $N = 600$ points, which showed that the solutions computed using $N = 400$ points were converged to graphical accuracy.

In order to verify this method, we considered the waveless flow over an ellipse. By specifying the Froude number and ellipse height, we were able to find ellipse lengths that resulted in waveless solutions and reproduce the contours as found by Forbes [9] and Hocking *et al.* [16].

5 Results

In order to find the contours of waveless solutions, we start with an initial guess of uniform flow and a flat free surface located at $y = 1$ and use this to find a solution for a small obstruction. We consider two Gaussian obstructions and our initial guess for the separation is that found using the linear methods, $b = \frac{(2k+1)\pi}{\alpha}$, $k = 0, 1, 2, \ldots$, where α is the positive real root of the transcendental equation, $\frac{\tanh\alpha}{\alpha} = F^2$. We then increase the height (or the depth if we are finding the contours for the trenches) by small steps using the solution from the previous height as the new initial guess. The separation is recorded at each height and contours are plotted showing the height and separation at which waveless solutions occur.

5.1 Contour behaviour

Contours were plotted for four different Froude numbers, $F = 0.5$, 0.55, 0.6 and 0.7, and are included in Figures 2–5 respectively. In these figures each of the circles represents a

https://doi.org/10.1017/S0956792512000381 Published online by Cambridge University Press

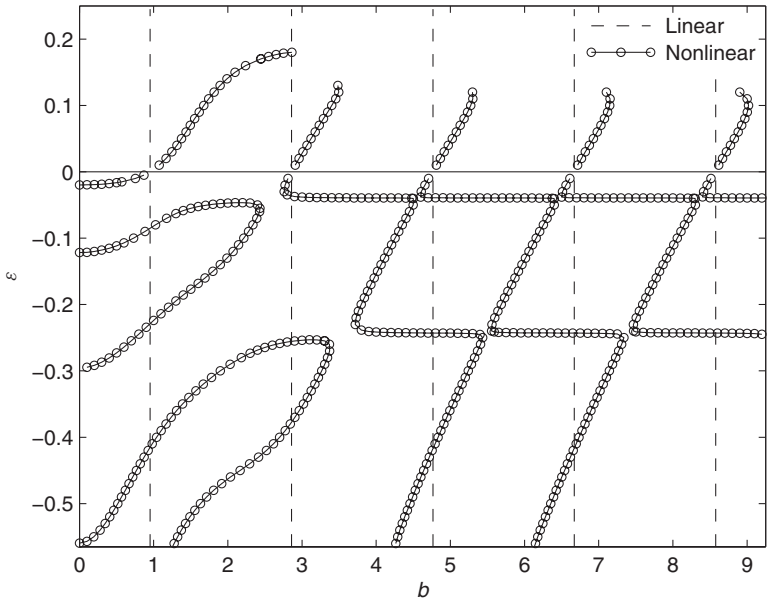

FIGURE 3. Contour plot showing the values of obstruction height and separation that result in waveless solutions for $F = 0.55$.

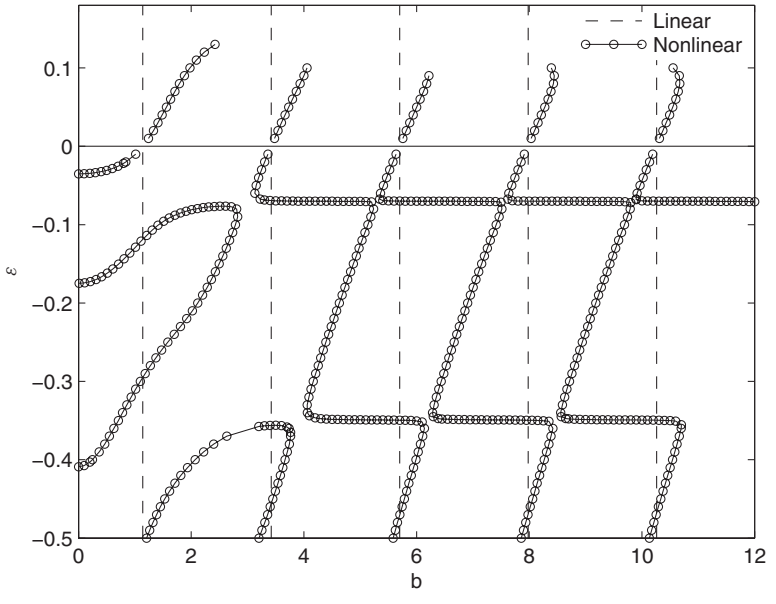

FIGURE 4. Contour plot showing the values of obstruction height and separation that result in waveless solutions for $F = 0.6$.

https://doi.org/10.1017/S0956792512000381 Published online by Cambridge University Press

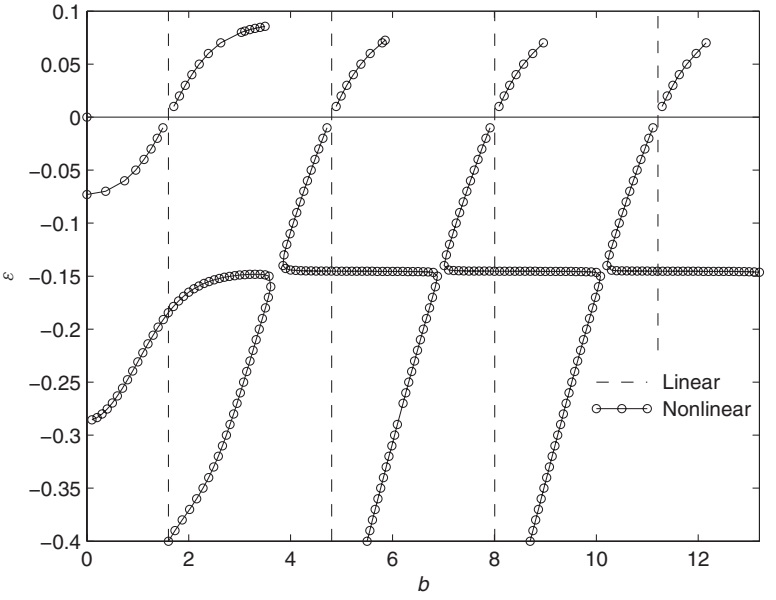

FIGURE 5. Contour plot showing the values of obstruction height and separation that result in waveless solutions for $F = 0.7$.

waveless solution to the nonlinear problem, while the dashed lines represent the separation values that result in waveless solutions in the linearised problem.

Considering the contours for obstructions of positive height, we observe that the first of the positive contours for the case $F = 0.5$ is fairly straight in the middle, with a slight curve near $\varepsilon = 0$ and starts to level off near the maximum height. This first contour seems to terminate when waves that can not be eliminated start to form on the surface both upstream and downstream of the object. As the Froude number is increased, the first positive contour straightens near $\varepsilon = 0$ and the maximum height reached decreases. The remaining positive contours are fairly straight, deviating from the linear values, until they curl over just before terminating. For the cases $F = 0.5$, 0.55 and 0.6, the tops of these positive contours curl towards $b = 0$, while those for $F = 0.7$ curl away from $b = 0$.

The contours for obstructions of negative height (or trenches) have quite different behaviour. There is a negative contour, which appears to continue from each of the positive contours, the first of which curves towards $b = 0$, while the remaining contours form a 'zig-zag' pattern, with each contour having a number of horizontal sections. There are also other contours present, which do not correspond to any of the positive contours and form loops that appear to originate from $b = 0$. These looped contours turn over at a depth corresponding with the turns at the beginning of each horizontal section in the second negative contour. As the Froude number is increased, the depths at which the first negative contour and the looped contours meet the ε-axis increase. Each of the horizontal sections of the contours also occurs at a larger depth, along with the tops of the looped contours.

We note that, particularly in the negative case, the contour behaviour is quite different at low separation values. The transition from two obstructions to one obstruction as

https://doi.org/10.1017/S0956792512000381 Published online by Cambridge University Press

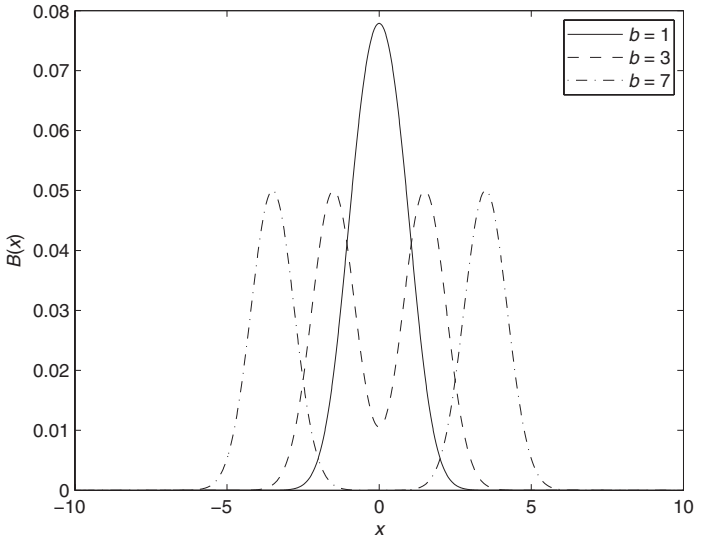

FIGURE 6. Obstructions $B(x)$ of height $\varepsilon = 0.05$ for three different separations, $b = 1$, 3 and 7. Note that for $b = 1$, the two objects merge into a single obstruction.

separation decreases, as observed in Figure 6, may explain the difference in the contour behaviour at these low separation values.

5.2 Solution behaviour: obstructions of positive height

The solutions for the free surface on the first of the positive contours have a dip above the obstruction that increases in depth as the obstruction increases in height. The solutions on the remaining contours have two dips, one above each obstruction, with a number of trapped waves in-between. The solutions on the second positive contour have one-half trapped wave, those on the third contour have one and a half trapped waves, those on the fourth have two and a half trapped waves and so on. Some of the solutions from the first four positive contours for $F = 0.5$ can be seen in Figure 7. This behaviour seems to be consistent across the four Froude numbers considered.

5.3 Solution behaviour: obstructions of negative height

The solutions from the trenches differ significantly on various contours and their branches. We will first consider solutions from negative contours which continue from their corresponding positive contours. The first negative contour, for each of the Froude numbers considered, has solutions that have a single peak which increases in height as the trench increases in depth. The remaining contours, which follow the 'zig-zag' pattern, will be broken down into 'downward' and 'horizontal' branches to describe the behaviour of solutions.

The first downward branch of each of the contours for the case $F = 0.5$ has solutions with two distinct peaks with no observable trapped waves in-between. This section ends at

https://doi.org/10.1017/S0956792512000381 Published online by Cambridge University Press

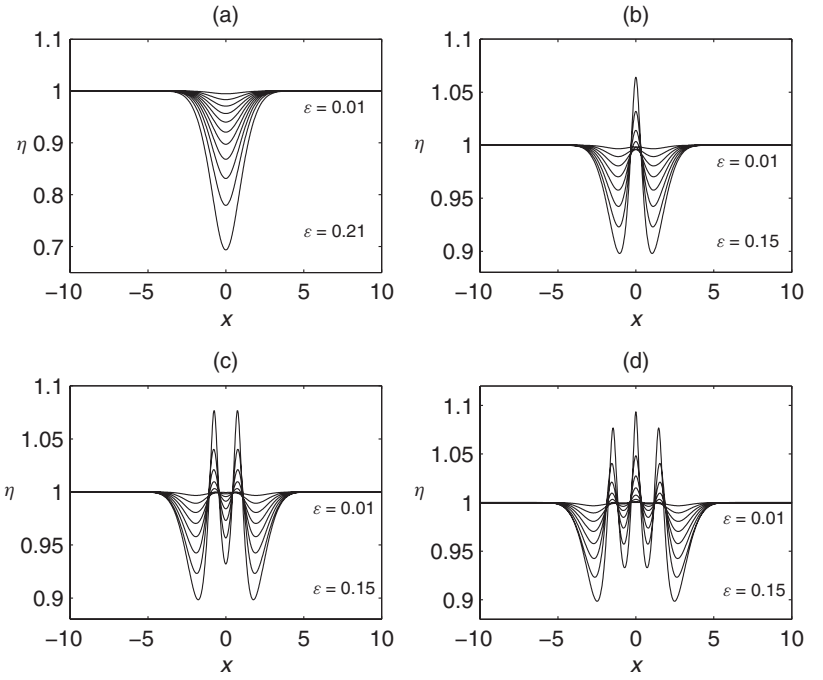

FIGURE 7. Waveless solutions for $F = 0.5$ from the first four positive contours. (a) shows solutions from the first positive contour, (b) shows solutions from the second positive contour, (c) shows solutions from the third and (d) shows solutions from the fourth positive contour. These solutions occur at values of ε evenly spaced between two values in each plot. Solutions in (a) have a dip directly above the obstruction, increasing in depth as the obstruction increases in height. Solutions in (b), (c) and (d) have a dip above each obstruction with a number of trapped waves in-between.

a very shallow depth and hence the solutions calculated were very close to the turn at the bottom of each branch and this may account for why no trapped waves were observed. For the cases $F = 0.55$, 0.6 and 0.7, the solutions from the first downward section of each of the contours have two distinct peaks which have a number of waves trapped between them which then flatten out as the solutions become closer to the depth at which the contour turns. For the $F = 0.55$ case, the second contour has no trapped waves, the third contour has one-half trapped wave, the fourth contour has one and a half trapped waves and the fifth contour has two and a half trapped waves. As the Froude number is increased, these trapped waves become greater in amplitude relative to the height of the peaks and also drop downward slightly so that the number of trapped waves increases. For the $F = 0.6$ and 0.7 cases, the second contour has one-half trapped wave between two peaks, the third contour has one and a half trapped waves, the fourth contour has two and a half trapped waves and the fifth contour has three and a half trapped waves. A comparison of solutions from the first section of the fourth negative contour for different Froude numbers is included in Figure 8.

In the four cases, i.e. $F = 0.5$, 0.55, 0.6 and 0.7, the solutions from the first horizontal section of each of the 'zig-zag' contours have two distinct peaks with a broad trough in-between. This trough widens as the separation between the trenches is increased.

https://doi.org/10.1017/S0956792512000381 Published online by Cambridge University Press

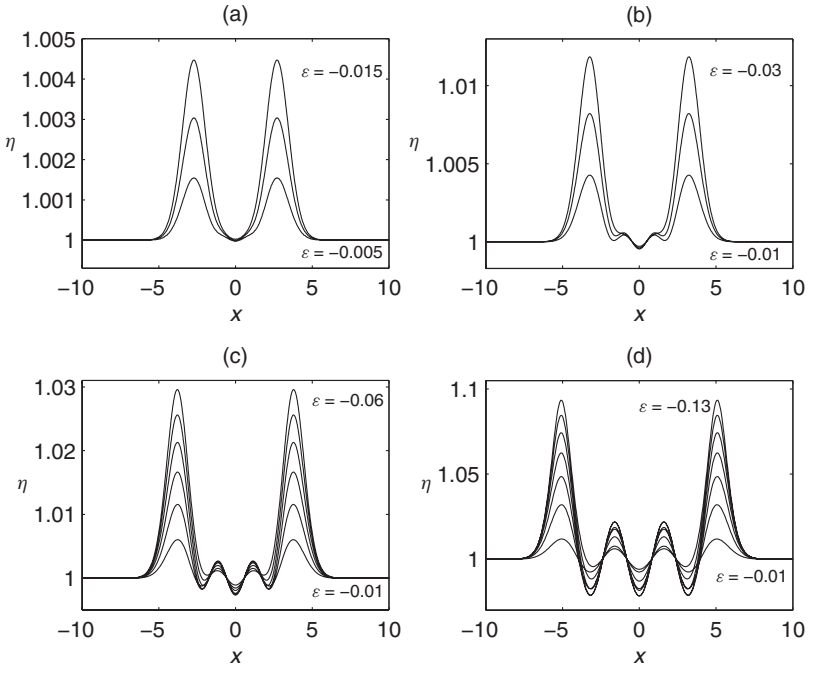

FIGURE 8. Comparison of solutions from the first downward branch of the fourth negative contour. (a) shows solutions for $F = 0.5$, (b) shows solutions for $F = 0.55$, (c) shows solutions for $F = 0.6$ and (d) shows solutions for $F = 0.7$. The values of ε are evenly spaced between two values in each plot. The solutions for $F = 0.5$ have two distinct peaks with no observable trapped waves in-between, while those for $F = 0.55$ have one and a half trapped waves. Solutions for $F = 0.6$ and 0.7 have two and a half trapped waves.

Solutions on the second downward branch of each of the 'zig-zag' contours for the case $F = 0.5$ have two distinct peaks and develop a number of trapped waves between the peaks which flatten out again by the turn at the bottom of the branch. The solutions on the second contour have no trapped waves, those on the third contour develop one-half trapped wave and those on the fourth contour develop one and a half trapped waves. For the $F = 0.55$, 0.6 and 0.7 cases, the solutions on the second downward branch develop one-half wave trapped at the top of each peak as the depth of trenches is increased. The solutions also develop a number of waves trapped between the peaks which flatten out again by the bottom of the branch. The number of trapped waves is consistent across the three cases, i.e. $F = 0.55$, 0.6 and 0.7; the solutions on the second negative contour develop one-half trapped wave, those on the third develop one and a half trapped waves and those on the fourth develop two and a half trapped waves. Figure 9 shows solutions from the second downward section of the second negative contour. We observe that for $F = 0.5$, the solutions have two distinct peaks, while those for $F = 0.55$ and 0.6 develop one-half wave trapped at the top of each peak. Note that for $F = 0.7$, one-half trapped wave also develops at the top of each peak, but this is not observed fully, as the largest amplitude solution plotted corresponds with the deepest point on the contour plot and not with the bottom of the branch. We also observe that for larger F, the depth of the

https://doi.org/10.1017/S0956792512000381 Published online by Cambridge University Press

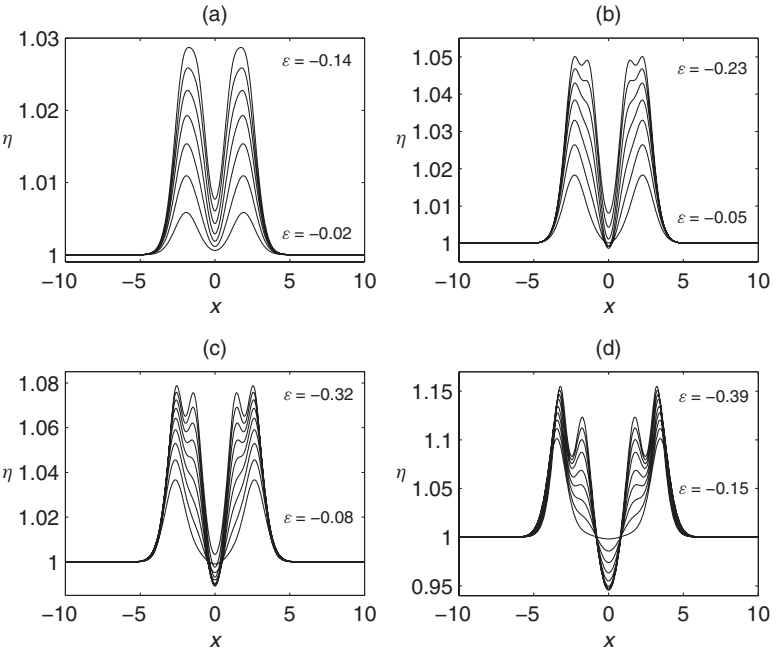

FIGURE 9. Comparison of solutions from the second downward branch of the second negative contour. Values of ε are evenly spaced between two values indicated in each plot. (a) shows solutions for $F = 0.5$, (b) shows solutions for $F = 0.55$, (c) shows solutions for $F = 0.6$ and (d) shows solutions for $F = 0.7$. Note that for $F = 0.7$, the largest depth solution plotted does not correspond with the bottom of the branch.

wave trapped at the top of the peak and the depth of the trough or trapped wave between the peaks are greater relative to the height of the peaks themselves.

Note that the contour plot for $F = 0.7$ does not include the branches past the second downward section, so will not be included in the discussion of lower branches.

For the cases $F = 0.55$ and 0.6, the solutions from the second horizontal section of each of the 'zig-zag' contours have two peaks with one-half wave trapped at the top of each peak and a broad trough in-between. This trough widens as the separation between the trenches is increased. The solutions for $F = 0.5$ differ as they do not have any waves trapped at the top of the peaks.

The solutions on the third downward section of the 'zig-zag' contours for the case $F = 0.5$ have a number of trapped waves between two peaks. These two peaks become narrow and distorted as the depth of trenches is increased. The solutions on the second contour have no trapped waves between the peaks and those on the third contour develop one and a half trapped waves between the peaks, which then flatten out again so that the solutions at the bottom of the branch have two peaks with a broad trough in-between. For the cases $F = 0.55$ and 0.6, the solutions in the third downward section develop one trapped wave at top of each peak. Solutions on the second contour develop one-half trapped wave between two peaks and those on the third contour develop one and a half trapped waves. The third downward section of the fourth negative contour is only

https://doi.org/10.1017/S0956792512000381 Published online by Cambridge University Press

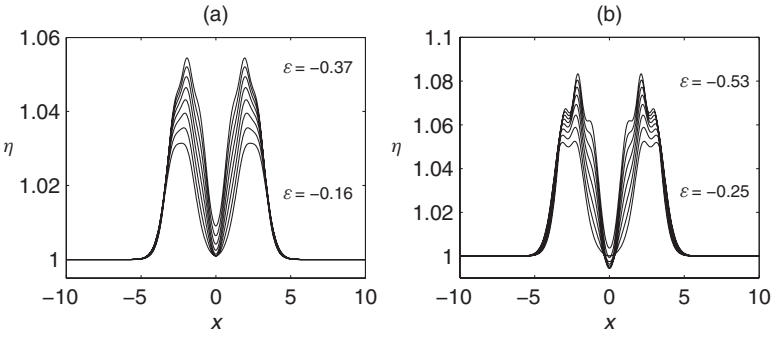

FIGURE 10. Comparison of solutions from the third downward section of the second negative contour. (a) shows solutions for $F = 0.5$ and (b) shows solutions for $F = 0.55$. ε values for solutions in each plot vary evenly between the two values indicated.

included in the case $F = 0.6$ and these solutions develop two and a half waves trapped between the peaks. A comparison of solutions from the third downward section of the second negative contour for the $F = 0.5$ and 0.55 cases is included in Figure 10.

We will now consider the behaviour of solutions on looped contours, which are those which do not appear to correspond with any of the positive contours and form loops that originate from the ε-axis. To better explain these solutions, we break these loops into 'upper' and 'lower' branches. The upper branch on each looped contour is taken from the shallower intersect with the ε-axis and followed upwards to the point at which the contour turns back on itself. The lower branch begins at this turn and follows the contour downwards to the deeper intersect with the ε-axis.

Included in Figure 11 are solutions from the looped contours for the $F = 0.5$ case. The solutions from the shallower loop are included with those from the upper and lower branches in Figures 11(a) and (b) respectively. The solutions from the upper and lower branches of the deeper loop are included in Figures 11(c) and (d) respectively. We note that the highest amplitude solution in each of the plots corresponds to the deepest point of each branch. In Figures 11(a), (b) and (c) this is the point at which the branch intersects the ε-axis. In Figure 11(d) the highest amplitude solution corresponds to the deepest point on the branch that was included in the contour plot. Due to the shape of the looped contours, the solutions in these plots are not evenly spaced in b or ε, but are instead chosen to best show the evolution of the solutions.

Following the shallower looped contour, starting from the ε-axis intersect of the upper branch, we observe that the solutions have a single peak which decreases in height and develops one-half wave trapped at the top of the peak. Once the contour turns into the lower branch, the peak increases in height and the half trapped wave flattens out. As we follow the contour further, a narrow distorted peak develops before the branch intersects with the ε-axis. The solutions from the deeper contour differ in that the upper branch begins with solutions that have one-half wave trapped at the top of a single narrow distorted peak. As we follow the upper branch away from the ε-axis, the half trapped wave increases in depth and the peak decreases in height, increases in width and the distortion disappears. Once the contour turns into the lower branch, the peak again

https://doi.org/10.1017/S0956792512000381 Published online by Cambridge University Press

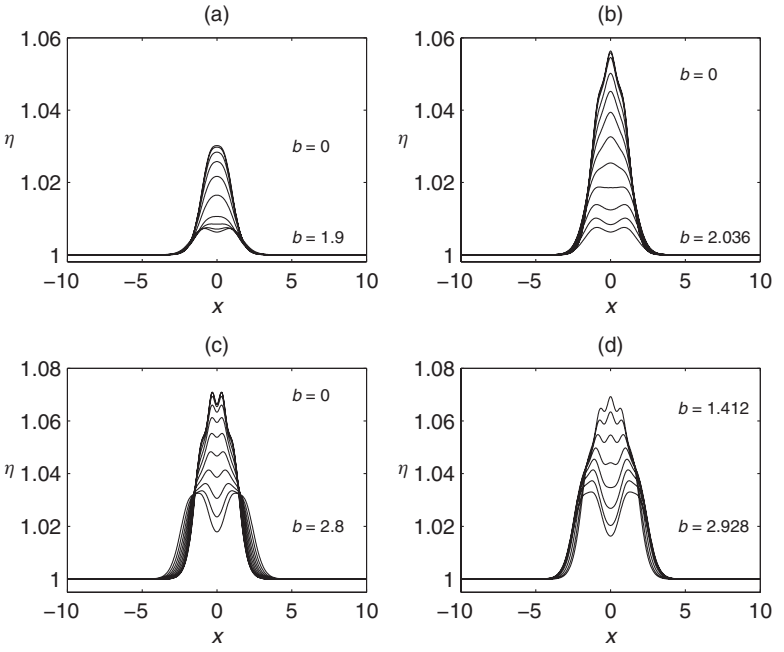

FIGURE 11. Solutions for $F = 0.5$ from the looped contours. The separation values for solutions vary between two b values indicated. These are not evenly spaced values of b, but are chosen to show the evolution of solutions as the separation changes. (a) shows solutions from the upper branch of the shallower contour and (b) shows solutions from the lower branch. (c) shows solutions from the upper branch of the deeper contour and (d) shows solutions from the lower branch. The highest amplitude solution in each of the plots corresponds to the deepest point on each branch.

increases in height, decreases in width, starts to become distorted and one and a half trapped waves start to develop. These trapped waves are not shown to develop fully as Figure 11 only includes the solutions corresponding to the points on the contour plot and not the full length of this branch.

Solutions from the looped contours for $F = 0.55$ are included in Figure 12. As before, the solutions from the upper and lower branches of the shallower contour are included in Figures 12(a) and (b) respectively and the solutions from the upper and lower branches of the deeper contour are included in Figures 12(c) and (d) respectively.

We observe that the solutions from the shallower loop for the $F = 0.55$ case have similar behaviour to those from the deeper loop for the $F = 0.5$ case but without distortion.

Following the deeper loop from the ε-axis intersect of the upper branch, we observe solutions with two and a half waves trapped at the top of a single peak which decreases in height and increases in width. The trough in the middle of the trapped waves increases in depth until solutions are observed that have two peaks with one-half wave trapped at the top of each peak and a shallow trough in-between. Once the contour turns into the lower branch, the peaks increase in height, decrease in width and the trough between the two becomes shallower and begins to develop one-half trapped wave. Following the contour further, the solutions begin to develop into three and a half waves trapped at the top of

https://doi.org/10.1017/S0956792512000381 Published online by Cambridge University Press

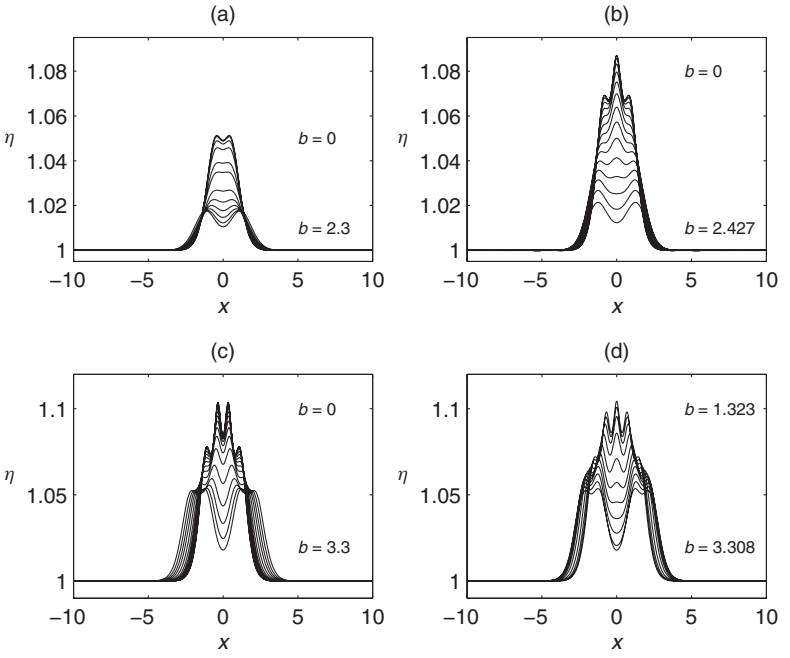

FIGURE 12. Solutions for $F = 0.55$ from the looped contours. The values of the separation vary between two b values indicated on each plot. These b values are not evenly spaced, but are instead chosen to best show the evolution of solutions. (a) shows solutions from the upper branch of the shallower contour and (b) shows solutions from the lower branch. (c) shows solutions from the upper branch of the deeper contour and (d) shows solutions from the lower branch. The highest amplitude solution in each of the plots corresponds with the deepest point on the contour plot from the corresponding branch.

a single peak. Again these waves are not shown to develop fully as only the solutions corresponding to the points included on the contour plot are included in Figure 12.

The solutions from the looped contours for the cases $F = 0.6$ and 0.7 are of similar form to those for the $F = 0.55$ case.

6 Conclusion

In this paper we have calculated waveless subcritical solutions for flow over two Gaussian obstructions of both positive and negative heights. Contours showing the obstruction height and separation at which these waveless solutions occur were plotted for four different Froude numbers. The contours of nonlinear solutions quickly deviated from the linear values as the obstruction height or trench depth was increased. The solutions for obstructions of positive height were of similar form for each of the four Froude numbers considered, but differed from the case of an ellipse on the stream bed and the results of [9] and [16] as the contours did not merge together.

The free-surface shapes for solutions for flow over two Gaussian trenches varied significantly over different Froude numbers, in both form of solutions and behaviour of contours, with various distorted wave shapes observed on a mosaic of branches.

https://doi.org/10.1017/S0956792512000381 Published online by Cambridge University Press

Interestingly, once the trenches separated into two distinct holes, the pattern became a kind of an 'ant farm' pattern, and in particular there were values of depth for which there were waveless solutions for all separations greater than some particular value. For example, at $F = 0.6$ there exist waveless solutions for $\varepsilon \approx -0.35$ for all values of $b > 4$. This may provide some design conditions for drag-free bottom flows.

References

[1] Baines, P. G. (1987) Upstream blocking and airflow over mountains. *Ann. Rev. Fluid Mech.* **19**, 75–97.

[2] Belward, S. R. (1999) Fully nonlinear flow over successive obstacles: Hydraulic fall and supercritical flows. *J. Aust. Math. Soc. Ser. B* **40**, 447–458.

[3] Binder, B. J., Dias, F. & Vanden-Broeck, J.-M. (2005) Forced solitary waves and fronts past submerged obstacles. *Chaos* **15**, 037106-1-13.

[4] Binder, B. J., Dias, F. & Vanden-Broeck, J.-M. (2008) Influence of rapid changes on free surface flows. *IMA J. Appl. Math.* **73**, 254–273.

[5] Choi, J. W. (2002) Free surface waves over a depression. *Bull. Aust. Math. Soc.* **65** 329–335.

[6] Dias, F. & Vanden-Broeck, J.-M. (2002) Generalised critical free surface flows. *J. Eng. Math.* **42**, 291–301.

[7] Dias, F. & Vanden-Broeck, J.-M. (2004) Trapped waves between submerged obstacles. *J. Fluid. Mech.* **509**, 93–102.

[8] Forbes, L. K. (1981) On the wave resistance of a submerged semi-elliptical body. *J. Eng. Math.* **15**, 287–298.

[9] Forbes, L. K. (1982) Non-linear, drag-free flow over a submerged semi-elliptical body. *J. Eng. Math.* **16**, 171–180.

[10] Forbes, L. K. (1985) On the effects of non-linearity in free-surface flow about a submerged point vortex. *J. Eng. Math.* **19**, 139–155.

[11] Forbes, L. K. (1988) Critical free-surface flow over a semi-circular obstruction. *J. Eng. Math.* **22**, 3–13.

[12] Forbes, L. K. & Schwartz, L. W. (1982) Free-surface flow over a semicircular obstruction. *J. Fluid Mech.* **114**, 299–314.

[13] Higgins, P. J., Read, W. W. & Belward, S. R. (2006) A series-solution method for free-boundary problems arising from flow over topography. *J. Eng. Math.* **54**, 345–358.

[14] Hocking, G. C. (2006) Steady Prandtl-Batchelor flows past a circular cylinder. *ANZIAM J.* **48**, 165–177.

[15] Hocking, G. C. & Forbes, L. K. (2001) Supercritical withdrawal from a two-layer fluid through a line sink if the lower layer is of finite depth. *J. Fluid Mech.* **428**, 333–348.

[16] Hocking, G. C., Holmes, R. J. & Forbes, L. K. (2012) A note on waveless subcritical flow past a submerged semi-ellipse. *J. Eng. Math.* (In press).

[17] Lamb, H. (1932) *Hydrodynamics*, 6th ed., Cambridge University Press, Cambridge, UK.

[18] Long, R. R. (1972) Finite amplitude disturbances in the flow of inviscid rotating and stratified fluids over obstacles. *Ann. Rev. Fluid Mech.* **4**, 69–92.

[19] Pratt, L. J. (1984) On nonlinear flow with multiple obstructions. *J. Atmos. Sci.* **41**, 1214–1225.

[20] Tuck, E. O. (1989) A submerged body with zero wave resistance. *J. Ship Res.* **33**, 81–83.

[21] Vanden-Broeck, J.-M. (1987) Free-surface flow over an obstruction in a channel. *Phys. Fluids* **30**, 2315–2317.

[22] Zhang, Y. & Zhu, S. (1996) Open channel flow past a bottom obstruction. *J. Eng. Math.* **30**, 487–499.

[23] Zhang, Y. & Zhu, S. (1996) A comparison study of nonlinear waves generated behind a semicircular trench. *Proc. R. Soc. Lond.* **452**, 1563–1584.